PCCP

PAPER

View Article Online
View Journal | View Issue

Cite this: *Phys. Chem. Chem. Phys.*, 2014, **16**, 12266

Optical and electrochemical properties of ethynylaniline derivatives of phenothiazine, phenothiazine-5-oxide and phenothiazine-5,5-dioxide†

Kim D. Thériault and Todd C. Sutherland*

Received 14th February 2014,
Accepted 25th April 2014

DOI: 10.1039/c4cp00678j

www.rsc.org/pccp

Three phenothiazine (PTZ) derivatives with varying degrees of sulfur oxidation states were synthesized as strong electron donors. The thioether, sulfoxide and sulfone PTZ-derivatives exhibited irreversible oxidation at 0.19 V, 0.29 V and 0.31 V *versus* ferrocene, respectively. Each PTZ derivative was emissive with lifetimes of 1.7 ns, 0.5 ns, and 0.5 ns and absolute quantum yields of 0.32, 0.23 and 0.23 for the thioether, sulfoxide and sulfone derivatives, respectively. Furthermore, these PTZ derivatives showed very large Stokes shifts ranging from 5600 cm^{-1} to 2800 cm^{-1}. Calculations using DFT and TD-DFT methods resulted in an optimized ground state and the excited state geometries of the PTZ derivatives that compared favourably to experimental optical and electrochemical data. DFT calculations revealed that these butterfly shaped derivatives flatten upon excitation and this effect is greatest for the thioether PTZ derivative, resulting in the large Stokes shift. These potent electron donor systems also displayed electrochromic behaviour upon oxidation, which was attributed to a delocalized cation over the phenothiazine core and the appended ethynyl anilines. The electrochemically oxidized species had a wide absorption profile spanning from 300 nm to past 800 nm.

Introduction

Phenothiazine (PTZ) has a long and rich history, beginning in the late 19th century of its use as a dye molecule,[1] such as Lauth's violet and methylene blue. PTZ derivatives regained popularity in pharmacology due to the reversal of multidrug resistance.[2,3] More recently, PTZ was explored as an organic semiconductor because it possesses a high lying HOMO energy and was considered as an electron-donating (p-type) building block.[4] Owing to its strong electron donating character, several synthetic derivatives of PTZ explored the electronic tunability by electron-donating and electron-withdrawing substituents for semiconductor applications.[5–8]

The PTZ core and its atom numbering are shown at the top of Scheme 1. Regioselective derivatization of PTZ has been extensively explored in the literature and the most common substituents are at the nitrogen and the 3,7-positions. Of the over one thousand 3,7-PTZ derivatives reported, there are only ten reports of PTZ derivatized with an alkyne functionality.[9–18] Our approach was to install electron rich functionality, *via* dialkylanilines, that are bridged through a conjugated spacer to enhance the donor capability of PTZ. The alkyne spacer was deemed as important to permit co-planarity between the aniline and the PTZ for more effective π-donation. The alkyne spacer should impart desirable optical effects due to the extended conjugation and may alter the electrochemical oxidation properties. The goal of this work is to explore these PTZ derivatives as candidate electrons donors for organic electronic applications. In addition, we investigated the effect of oxidizing the sulfur in the thiazine ring to potentially access intramolecular donor–acceptor electronic interactions, as observed in phenoxazine[19] and dibenzoazaborine[20,21] systems.

Structurally, the thiazine heterocycle of PTZ is non-planar and several researchers have solved single-crystal X-ray structures showing that the angle between planes of the annulated benzo groups range from 138 to 156 degrees.[22–28] The angle between planes of the annulated benzo groups of the congeners typically widens with increasing oxidation of the sulphur: 145 to 162 degrees for the sulfoxide[22,26,29–34] and 134–163 degrees for the sulfone.[23,32,33,35–37] However, there is significant overlap between angle ranges and the different sulfur oxidation states, implying that the thiazine ring is rather flexible and its structure is determined by both synthetic derivatization and crystal packing. Interestingly, the non-planar thiazine ring in PTZ is speculated to be responsible for the large Stokes shifts observed in the fluorescence spectra.

Department of Chemistry, University of Calgary, 2500 University Drive NW, Calgary Alberta, Canada. E-mail: todd.sutherland@ucalgary.ca; Fax: +1 403 289 9488; Tel: +1 403 220 7559

† Electronic supplementary information (ESI) available: Calculated geometries of ground and excited states; cyclic voltammograms; differential pulse voltammograms; FTIR spectra; ^{1}H and ^{13}C NMR spectra; fluorescence lifetime measurements. See DOI: 10.1039/c4cp00678j

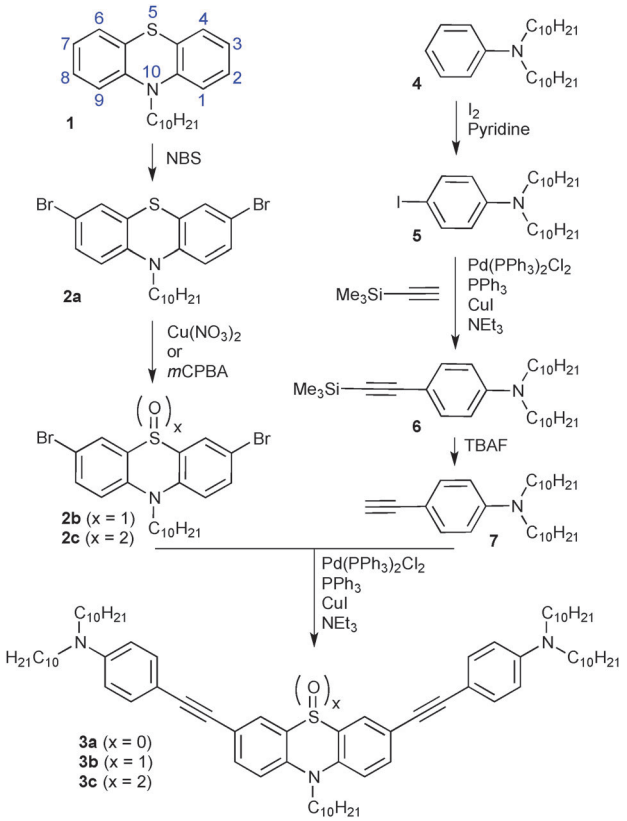

Scheme 1 Synthesis of ethynylaniline PTZ oxides **3a–3c**.

Here we present the synthesis of three bis-alkynylaniline PTZ derivatives, shown in Scheme 1, with the sulfur of the thiazine ring in the S(II), S(IV) and S(VI) oxidation states. The effects of the different sulfur oxidation states are explored using optical absorption spectroscopy, fluorescence spectroscopy, electrochemistry and spectroelectrochemistry and the results are interpreted by comparison to DFT-calculations. Appending dialkyl ethynylanilines to the PTZ core gives organic soluble building blocks that could lead to uniform thin films.

Results and discussion

Synthesis

The synthesis of the ethynylaniline-PTZs, shown in Scheme 1, begins with *N*-alkylating PTZ under the typical conditions reported by Sailer.[38] We elected to install decyl chains early in the synthesis to aid in organic solubility for subsequent purification steps. Regioselective electrophilic bromination also followed methods in the literature[39,40] to give 3,7-dibrominated precursor **2a** in modest yields. The PTZ core building block **2a** was subjected to either mild (Cu^{2+}) or strong (*m*CPBA) oxidizing conditions, which resulted in sulfur oxidation to PTZ-5-oxide **2b**[41] or PTZ-5,5-dioxide **2c**.[42] The three different sulfur oxidation states of PTZ (**2a–2c**) were finally reacted under Sonogashira conditions with *N*,*N*-didecyl-4-ethynylaniline to give PTZ derivatives **3a** to **3c**, which are highly soluble in common organic solvents.

Optical properties

The absorption and fluorescence spectra of **3a** to **3c** in CH_2Cl_2 are shown in Fig. 1 and relevant optical data are summarized in Table 1. All three PTZ derivatives show intense optical transition from 400 nm and below. Both PTZ sulfoxide and sulfone (**3b** and **3c**) show near superimposable absorption spectra, whereas compound **3a** has a different absorption profile. Clearly, the sulfur oxidation state has an effect on the intensity of the optical transitions. PTZ **3a** has the lowest energy absorption onset, calculated by the intersection between absorption and fluorescence, at 2.8 eV compared to both sulfoxide **3b** and sulfone **3c** at 3.0 eV. Each PTZ derivative is moderately fluorescent in solution with quantum yields of 0.32 for **3a** and 0.23 for both **3b** and **3c**. The fluorescence lifetime of **3a** is the longest at 1.7 ns, while **3b** and **3c** have similar lifetimes of 0.5 ns.

Most notable in the emission of **3a** is the large Stokes shift of 5600 cm^{-1} as compared to **3b** and **3c** with Stokes shifts of 2800 cm^{-1} and 2900 cm^{-1}, respectively. Such a large Stokes shift for PTZ derivatives has been reported previously[43,44] and is attributed to a significant structural change occurring in the S_1 energy surface. The large change in structure is presumably the result of the bent ground-state structure becoming more planar in the excited state. Here, we postulate that the oxidation of the sulfur hinders the PTZ excited states from adopting the more planar structure, which results in a smaller Stokes shift for **3b** and **3c**, and these optical and structural properties are discussed further in the computational section.

A closer examination of the fluorescence spectrum of **3a** shows a distinct peak and a lower energy shoulder, which are

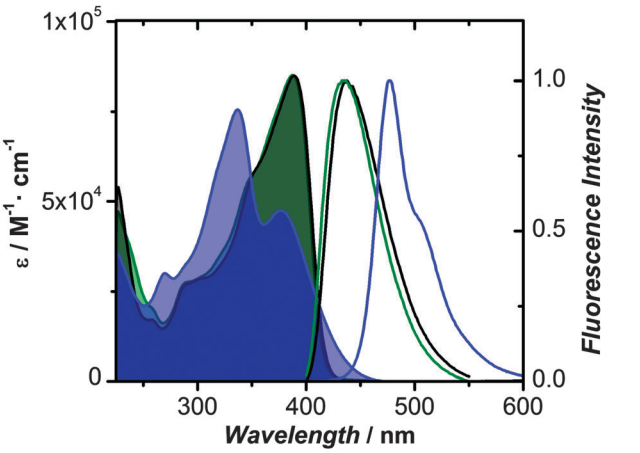

Fig. 1 Absorption and fluorescence spectra of **3a** (blue), **3b** (green) and **3c** (black) in CH_2Cl_2. Excitation for the fluorescence spectra was set at the lowest energy absorption band.

Table 1 Optical properties of **3a–3c**

Entry	λ_{max}/ nm (eV)	λ_{em}/ nm (eV)	Stokes shift/ cm^{-1}	τ/ns	ϕ
3a	377 (3.2)/337 (3.7)	477 (2.6)/504 (sh)	5600	1.7	0.32
3b	388 (3.2)/348 (sh)	435 (2.9)	2800	0.5	0.23
3c	388 (3.2)/348 (sh)	438 (2.9)	2900	0.5	0.23

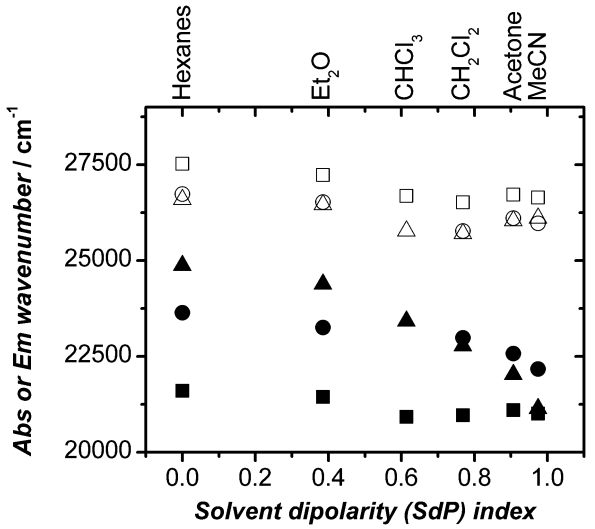

Fig. 2 Solvatochromic properties of lowest energy absorption (hollow points) and emission (solid points) bands for PTZs **3a** (squares), **3b** (circles) and **3c** (triangles) using the dipolarity index.

attributed to a vibronic side band with 1100 cm^{-1} energy spacing. The presence of vibronic bands in the fluorescence spectrum of **3a** supports the notion of a more planar or rigid structure. The absorption spectra of both **3b** and **3c** also show vibronic shoulders and peaks in the lowest energy region with an energy spacing of 2800 cm^{-1}.

Both the lowest energy absorption and emission peaks of PTZs **3a** to **3c** show solvatochromic effects, as depicted in Fig. 2. The absorption energy is highest in low polarity solvents, such as hexanes, and lowest in a moderate polarity CH_2Cl_2 solvent and again increases absorption energy in the polar acetonitrile. The absorption bands shift by approximately 1000 cm^{-1} over the range of solvents examined. The emission profiles of **3a** to **3c** show different solvatochromic behaviours. PTZ **3a** displays small perturbations over the solvent range ($\Delta\nu_{em}$ = 630 cm^{-1}), whereas sulfone PTZ, **3c**, exhibits a large spectral response to different solvents that span approximately 3700 cm^{-1}. PTZ **3b** shows intermediary solvatochromic emission relative to **3a** and **3c**. We have elected to use the solvent dipolarity (SdP) empirical scale, as described by Catalán,[45] to plot the absorption and emission peaks, as shown in Fig. 2. The SdP scale gave the most linear correlation to the absorption and emission peak data. Clearly, the single-parameter SdP scale does not adequately describe the complexities of the solvent interactions. Solvent effects can be divided into two interactions – specific and non-specific. Several solvent scales have been parameterized to describe the specific donor–acceptor interactions, such as Catalán's SA[46] and SB[47] scales, Kamlet and Taft's α and β,[48,49] Gutman's AN and DN scales[50] and Drago's E_B and C_B[51] scales to name a few. Non-specific interactions where the solvent is treated as a dielectric continuum were originally modelled by Kirkwood[52] and Onsager,[53] and have been empirically parameterized by the Dong and Winnik's Py scale,[54] Kamlet, Abboud and Taft's π^* scales,[55] Drago's S′ scale[56] and Catalán's SPP scale.[57] Many of the single parameter solvent scales were attempted here and resulted in poor linearity for both the absorption and emission peaks. The ESI† contains the absorption and emission spectral data for all the solvents and plots of two solvent scale approaches to demonstrate the limitations of the single-parameter solvent models in this PTZ system.

Instead, using Catalán's approach,[45] which combines two specific scales (SA and SB) and two general scales (SP and SdP) a multi-parameter, general approach was achieved to describe the solvent interactions for both the absorption and emission peaks. The detailed results of the fitting using the multi-parameter approach is found in the ESI,† but the highlights are described herein. All of the absorption peak data could be fitted with non-specific scales, solvent polarizability (SP) and solvent dipolarizability (SdP), with R^2 values of 0.94 or greater. Interestingly, the emission data required the inclusion of a solvent specific scale, solvent basicity (SB), in addition to the non-specific SP and SdP terms to induce reasonable fits to the emission data with R^2 values of 0.98 or greater. The SB term increased in significance in concert with the sulfur oxidation state in the thiazine ring, suggesting specific solvent to sulfur interactions in the excited state structure that are not present in the ground-state.

Electrochemical properties

All three PTZ derivatives show irreversible oxidation reactions in DMF using cyclic voltammetry, as shown in the ESI† and no reduction reactions were observed within the solvent stability potential window. Oxidation potentials are reported *versus* an internal ferrocene/ferricenium redox reaction using differential pulse voltammetry (DPV). PTZ derivatives **3a** to **3c** show increasing oxidation potentials of 190 mV, 285 mV and 310 mV, respectively. The stepwise increment in the oxidation potential is consistent with the change in the oxidation state of sulfur and stabilization of the HOMO with electron withdrawing groups. For comparison, the TMS-protected ethynyl aniline precursor shows an oxidation potential of 400 mV under the same electrochemical conditions. PTZ, under the same conditions, gives an oxidation potential of 150 mV, which is even lower than **3a** suggesting that the ethynyl anilines act as electron withdrawing groups in these compounds. That no reduction peaks were observed within the solvent stability window suggests that the change in sulfur oxidation state on the thiazine ring has minimal effect on lowering the LUMO energy.

Computations

Truncated models of the three final PTZ derivatives (Me groups replaced alkyl chains) were investigated using Density Functional Theory (DFT) and time-dependent (TD)-DFT calculations including solvent effects of the polarisable continuum model (PCM) at the B3LYP/6-31G+(d) level. Computational results using Gaussian09[58] with dichloromethane as the solvent provide insight into the absorption and emission energies and provide key insight into the structural changes following excitation.

All of the optimized ground state structures are butterfly-shaped about the thiazine ring, as shown in Fig. 3. Note the sulfoxide derivative has two possible thiazine ring conformations: S–O bond boat-axial (**3b$_{ax}$**) and S–O bond boat-equatorial (**3b$_{eq}$**).[29] Calculations show a small energetic preference of 8.3 kJ mol^{-1}

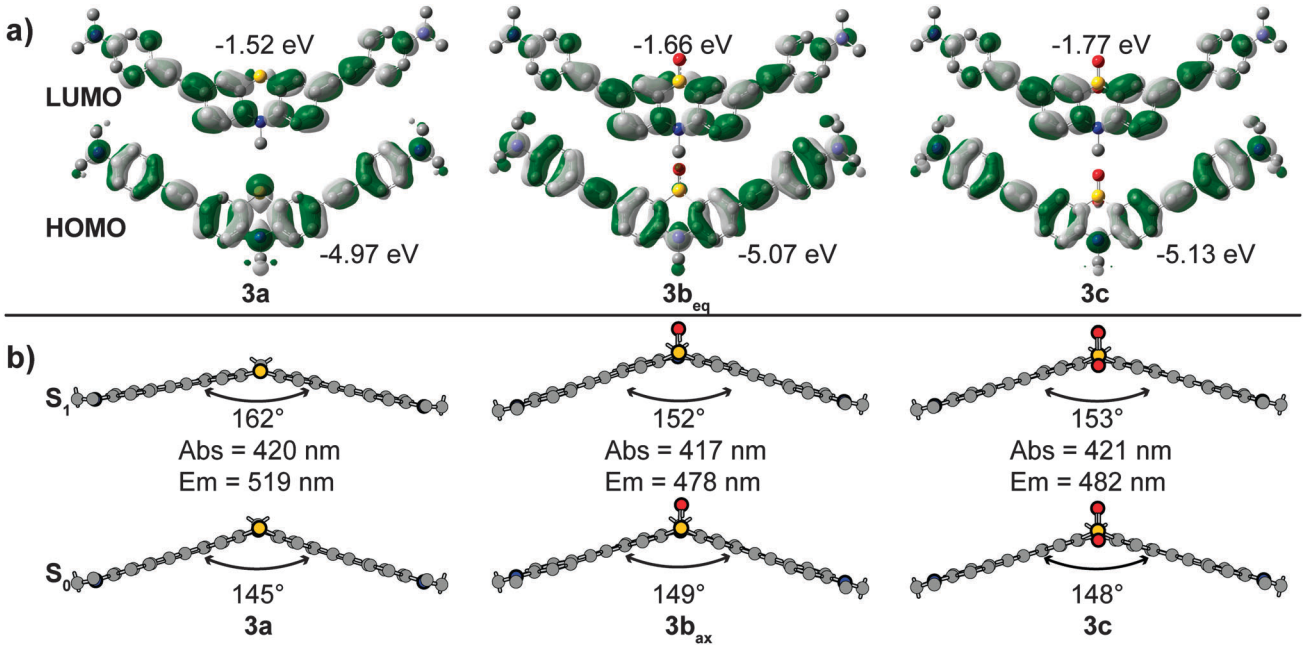

Fig. 3 (a) DFT optimized ground state structures of **3a**, **3b$_{eq}$** and **3c**, their FMOs and orbital energies using the B3LYP/6-31G+(d,p) basis set. (b) TD-DFT, using the same functional and basis set, calculations of S_0 and S_1 structures of **3a**, **3b$_{ax}$** and **3c** and their associated calculated absorption and emission peak energies.

for the axial S–O isomer and FT-IR results, included in the ESI,† were inconclusive as to the isomer formed upon oxidation. The optimized ground-state structure exhibited angles between planes (calculated by the intersection of the two imaginary planes extending from the annulated benzo groups) of 145°, 141°, 149° and 148° for **3a**, **3b$_{eq}$**, **3b$_{ax}$** and **3c**, respectively, as depicted in Fig. 3b. In addition, the optimized ground-state geometry resulted in dipole moments of 2.12 D, 7.69 D and 7.40 D, for **3a**, **3b$_{ax}$** and **3c**, respectively.

The FMOs and orbital energies are shown in Fig. 3a. The thiazine derivative, **3a**, has the highest HOMO energy of the series, as expected for such an electron-rich species. There is a decrease in the HOMO energy when oxidizing to the sulfoxide and a further HOMO stabilization upon sulfone generation, leading to an overall HOMO tunability range of 0.16 eV. The limited range of HOMO energy tunability over the series of PTZs likely reflects the delocalized contributions from the ethynyl-anilines. The HOMO coefficients of PTZs **3a** to **3c** are representative of a delocalized π-system over the entire conjugated system. Of notable difference is the coefficient on the sulfur atom in PTZ **3a**, whereas both **3b** and **3c** have nodes on sulfur. A similar decreasing energy trend in LUMO energies is found through the series of **3a** to **3c**. The LUMO shapes of **3a–3c** are nearly identical showing π-delocalized systems with nodes at both the nitrogen and sulfur atoms of the thiazine ring. The HOMO energy levels for **3a**, **3b$_{eq}$**, **3b$_{ax}$** and **3c** using DFT methods are −4.97 eV, −5.07 eV, −5.08 eV and −5.13 eV *versus* vacuum, respectively, compare favourably to the electrochemically-determined HOMO energy levels at −5.0 eV, −5.1 eV and −5.1 eV (using Fc/Fc^+ redox standard at −4.8 eV),[59] for **3a** to **3c**.

TD-DFT calculations using DCM as a solvent resulted in strong and exclusive HOMO to LUMO transitions in all three PTZ derivatives. The energies of the absorption transitions (S_0 to S_1) were approximately 420 nm (3.0 eV) for all of the PTZ derivatives, which is slightly lower in energy than the experimental values for **3a–3c** at 3.2 eV, determined by the λ_{max} value. The first excited state structure, S_1, was then optimized in the presence of DCM and additional TD-DFT calculations were carried out to assess the emission energy. Fig. 3b summarizes the results of the TD-DFT calculations and highlights the structural changes that occur in the first excited states following literature calculation methods.[60,61]

All three PTZ derivatives exhibit significantly red-shifted emission energies compared to the absorption energies, which supports the results of the experimentally observed Stokes shifts. Although, the absolute energy values are not directly comparable to the experimental values, the same trend is apparent and the computations provide insight into the associated structural changes in the excited states. The first singlet excited state (S_1) structure of PTZ **3a** is significantly more planar compared to its ground-state, S_0, structure, which is consistent with the largest Stokes shift in the series and appearance of vibronic bands in the fluorescence spectrum. The boat geometry of the thiazine ring changes from 145° to 162° in **3a**. For PTZ **3b**, both boat S–O axial and equatorial structures were computed in S_0 and S_1 states. Interestingly, only the axial structure **3b$_{ax}$**, mirrored both the absorption and emission experimental data, supporting the notion that the Cu-mediated oxidation mechanism yields exclusively the axial product. The boat geometry of the **3b$_{ax}$** thiazine oxide ring changes from 149° to 152°. The S_0 and S_1 structures of the S–O boat equatorial derivative, **3b$_{eq}$**, as calculated by DFT methods showed absorption and emission peaks at 418 nm and 497 nm, respectively. The ground state geometry

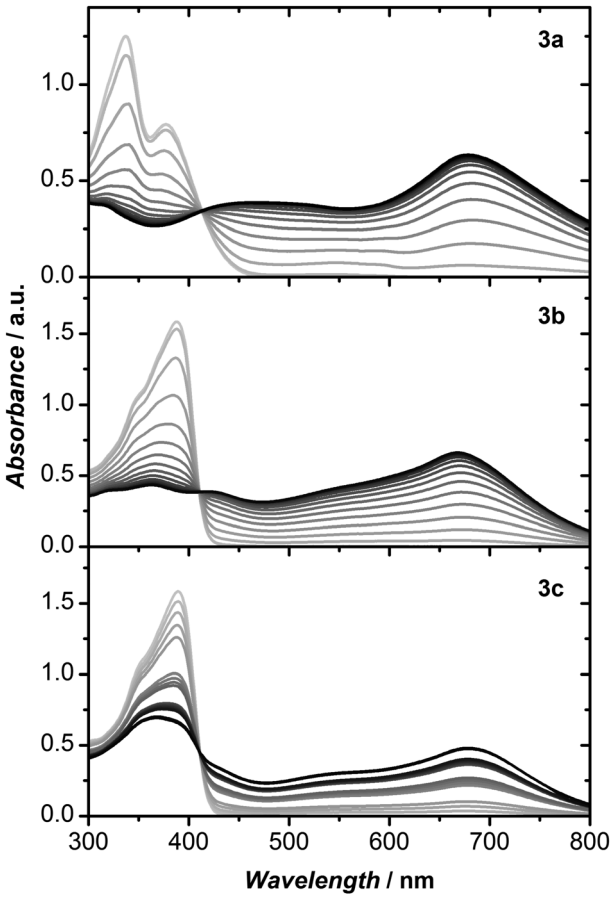

Fig. 4 Spectroelectrochemical evolution of the **3a–3c** (*ca.* 10^{-5} M in DMF) upon application of an oxidizing potential at the onset of oxidation determined from CV experiments. Each spectrum is taken at 1 minute intervals and the initial spectrum is a grey line that evolves to a black line over the time course of the experiment.

of $\mathbf{3b_{eq}}$ is very similar to the $\mathbf{3b_{ax}}$ derivative; however, the S_1 optimized structure of $\mathbf{3b_{eq}}$ is more planar than the S–O axial structure leading to a significant red-shift in emission, which the experimental data do not support. Clearly, the boat axial S–O of $\mathbf{3b_{ax}}$ inhibits the planarization of the PTZ leading to a smaller Stokes shift compared to that of **3a**. The optimized S_0 and S_1 structures of PTZ dioxide, **3c**, behaves very similarly to $\mathbf{3b_{ax}}$ with a change in the boat thiazine dioxide ring geometry of 148° to 153° upon excitation. The excited-state dipole moments of **3a**, $\mathbf{3b_{ax}}$ and **3c** are expectedly lower due to planarization than the S_0 structures at 0.87 D, 7.34 D and 6.79 D, respectively. Upon generation of the S_1 state, there is a contraction of the thiazine of both the N–C and S–C bonds, which we speculate helps in planarization, as has been described previously in the radical cation structure of PTZ.[62]

Spectroelectrochemistry

All three final PTZ derivatives are electron donors in addition to being highly conjugated; consequently, their absorption profile changes during the oxidation reaction were investigated. The evolutions of the absorption spectra for **3a** to **3c** are shown in Fig. 4. Each PTZ derivative shows the growth of an intense, red-shifted absorption profile that spans from 300 nm to over 800 nm, which is consistent with a highly delocalized cation charge. PTZ **3a** shows the most intense absorption with a broad peak centred at 680 nm. Compounds **3b** and **3c** share a similar absorption profile with peaks at 670 nm and 680 nm, respectively. Each absorption spectrum shown in Fig. 4 was recorded at 1 minute intervals for approximately 20 minutes. Clear isosbestic points are observed in each set of spectra at approximately 412 nm, which suggests either a stable radical cation that is electrochemically irreversible, or a chemical reaction following the electrochemical oxidation to form a new optically-active compound.

Most importantly, because these alkyne anilines are able to stabilize the oxidized PTZ to such a great extent these oxidized species could find applications into potent low energy photon absorbing materials, electrochromics or as p-type molecular candidates in organic electronic applications.

Conclusions

We have successfully synthesized an alkynyl aniline-PTZ adduct by exploiting Sonogashira reaction conditions to produce a set of potent electron donating, p-type, organic semi-conductor candidates. Optically, the neutral PTZ derivatives show modest absorption properties (<450 nm), but all derivatives are strongly emissive with large Stokes shifts of up to 5600 cm^{-1} and both absorption and emission peaks are solvatochromic. All three donors exhibited irreversible oxidation potentials as low as 0.19 V *vs.* Fc/Fc^+ and none of the PTZ derivatives displayed reductions within the solvent window, despite chemical oxidation to the thiazine-dioxide. TD-DFT calculations and optimizations show a reasonable correlation with experimental data and indicate that the PTZ derivatives become more planar in the excited state, rationalizing the large Stokes shift. Furthermore, the computationally-derived optical spectra support the S–O boat axial isomer over the equatorial S–O isomer. Upon electrochemical oxidation, all PTZ-derivatives exhibited a dramatic colour change owing to the delocalized cation through the PTZ core and appended ethynyl anilines that resulted in its absorption profile spanning from 300 nm to over 800 nm.

Experimental section

Materials

All chemicals were purchased from Aldrich and used as received without further purification, aside from the following: aniline was purchased from BHD, K_2CO_3 was purchased from EMD and $Pd(PPh_3)_2Cl_2$ was purchased from Strem. Solvents were used as received or dried using an MBraun solvent purification system. THF, DMF and DCM were stored over sieves before use and triethylamine was distilled in the presence of CaH and stored over sieves. Column chromatography was performed on a SiliCycle SilicaFlash P60 silica gel (230–400 mesh). Thin-layer chromatography was carried out on Merck silica gel F_{254} aluminium-backed TLC plates.

General

NMR spectra were recorded on a Bruker 400 MHz spectrometer and referenced to residual $CHCl_3$ in $CDCl_3$ (^{1}H 7.26 ppm, ^{13}C 77.00) or residual $(CH_3)_2CO$ in $(CD_3)_2CO$ (^{1}H 2.05 ppm). Mass spectra were recorded with an Agilent 6520 LC Q-TOF spectrometer run in ESI mode by direct infusion with the column bypassed. All samples were dissolved in DCM and run with an eluent flow rate of 0.2 mL min^{-1} MeOH, source temperature of 200 °C, fragmenter voltage of 120 V, Nebulizer pressure of 12 psi and a drying gas flow rate of 7 L min^{-1}. FTIR spectra were recorded in diffuse reflectance mode with drop-cast films on ground KBr on a Varian FTS-7000 spectrometer. UV/Vis spectra were recorded using a Cary 5000 spectrophotometer in dual beam mode. Emission spectra were recorded using a Photon Technology International (PTI) Quanta Master spectrofluorimeter operated in CW mode, with samples in a quartz Suprasil cell (1 cm width and path length, Hellma, Canada). Lifetime measurements were obtained at room temperature using an Edinburgh Instruments FLS920 spectrometer equipped with Fianium SC400 Super Continuum White Light Source, Hamamatsu R3809U-50 Multi Channel Plate detector and data were analyzed using Edinburgh Instruments F900 software. Curve fitting of the data was performed using a non-linear least squares procedure in the F900 software. Absolute fluorescence quantum yield values were measured using an Edinburgh Instruments FLS92 calibrated integrating sphere S 3 system.

4: *N,N*-Didecylaniline. Potassium carbonate (3.0640 g, 32.9 mmol) and 1-bromodecane (25 mL, 120.8 mmol) were added to a solution of aniline (3 mL, 32.9 mmol) in DMF (100 mL) and refluxed overnight. A blue colour appeared during the reaction but disappeared after completion. The solid residues were removed by filtration followed by removal of solvent *in vacuo*. The crude product was then reconstituted in diethyl ether, washed with water and the organic fraction was dried with magnesium sulfate. Removal of solvent *in vacuo* afforded a golden oil, which was purified by silica gel column chromatography (DCM) and resulted in a light yellow oil (11.7821 g, 95.8%).

5: *N,N*-Didecyl-4-iodoaniline. A solution of **4** (11.6409 g, 31.2 mmol) in dioxane : pyridine (1 : 1, 280 mL) was cooled in an ice bath. Iodine (19.1842 g, 75.6 mmol) was then added and the reaction mixture was stirred for 1 hour. Unreacted iodine was removed with saturated aqueous sodium thiosulfate (250 mL). Water (250 mL) was added to the organic fraction, then the product was extracted with DCM, dried with magnesium sulfate and the solvent was removed *in vacuo* to afford a blue oil as the crude product. Further purification with silica gel column chromatography hexanes : DCM (4 : 1) yielded **5** as a light yellow oil (12.1775 g, 78.2%). ^{1}H NMR (400 MHz, $CDCl_3$) δ 7.46 (d, J = 9.1 Hz, 2H), 6.46 (d, J = 9.1 Hz, 2H), 3.30–3.23 (m, 4H), 1.66–1.55 (m, 4H), 1.43–1.29 (m, 28H), 0.97 (t, J = 6.9 Hz, 6H). ^{13}C NMR (101 MHz, $CDCl_3$) δ 147.70, 137.72, 114.13, 75.53, 51.12, 32.04, 29.80, 29.78, 29.75, 29.73, 29.72, 29.70, 29.68, 29.66, 29.49, 29.48, 29.47, 29.45, 29.45, 27.29, 27.27, 27.21, 22.83, 14.26, 14.24. MS (ESI HRMS) m/z calcd for $C_{26}H_{47}IN$ + H: 500.2748; found 500.2734.

6: *N,N*-Didecyl-4-((trimethylsilyl)ethynyl)aniline. A yellow mixture of **5** (9.2376 g, 18.5 mmol), bis(triphenylphosphine)palladium(II) dichloride (0.6343 g, 0.90 mmol), triphenyl phosphine (0.7295 g, 2.78 mmol) and copper(I) iodide (0.3893 g, 2.04 mmol) in dry triethylamine (50 mL) was purged with N_2. Trimethylsilylacetylene (5.3 mL, 37.2 mmol) was added by syringe over 20 minutes. The reaction mixture was stirred at room temperature and under N_2 overnight. The solvent was removed from the brown mixture *in vacuo* and the crude product was purified using silica gel chromatography hexanes : DCM (1 : 1) to give **6** as an orange oil (8.4001 g, 96.7%). ^{1}H NMR (400 MHz, $CDCl_3$) δ 7.35 (d, J = 9.0 Hz, 2H), 6.56 (d, J = 9.0 Hz, 2H), 3.34–3.24 (m, 4H), 1.68–1.55 (m, 4H), 1.47–1.29 (m, 28H), 0.98 (t, J = 6.9 Hz, 6H), 0.31 (s, 9H). ^{13}C NMR (101 MHz, $CDCl_3$) δ 148.07, 133.32, 111.10, 108.96, 107.03, 90.61, 51.00, 32.05, 29.79, 29.72, 29.65, 29.48, 27.33, 27.24, 22.82, 14.22, 0.37. MS (ESI HRMS) m/z calcd for $C_{31}H_{56}NSi$ + H: 470.4177; found 470.4162.

7: *N,N*-Didecyl-4-ethynylaniline. A solution of TBAF (21 ml, 1 M in THF) was added to a solution of **6** (8.4001 g, 16.8 mmol) in DCM (25 mL) and the mixture was stirred at room temperature for 1 hour. The mixture was then washed with brine and H_2O, dried with magnesium sulfate and reduced *in vacuo* to obtain the crude product as a brown oil. The product was purified with silica gel column chromatography hexanes : DCM (1 : 1) to afford **7** as an orange oil (6.0262 g, 90.1%). ^{1}H NMR (400 MHz, $CDCl_3$) δ 7.35 (d, J = 8.9 Hz, 2H), 6.55 (d, J = 9.0 Hz, 2H), 3.31–3.24 (m, 4H), 2.97 (s, 1H), 1.64–1.54 (m, 4H), 1.40–1.25 (m, 28H), 0.92 (t, J = 6.8 Hz, 6H). ^{13}C NMR (101 MHz, $CDCl_3$) δ 148.34, 133.47, 111.19, 107.67, 85.21, 74.49, 51.08, 32.04, 29.80, 29.71, 29.66, 29.47, 27.34, 27.27, 22.82, 14.24. MS (ESI HRMS) m/z calcd for $C_{28}H_{48}N$ + H: 398.3781; found 398.3770.

1: 10-Decyl-10*H*-phenothiazine. A mixture of phenothiazine (5.1028 g, 25.6 mmol) and potassium *tert*-butoxide (3.1200 g, mmol) in dry THF (50 mL) was purged with N_2 before adding 1-bromodecane (10.4 mL, 50.3 mmol). The mixture was refluxed under N_2 overnight. Removal of the solids residues by filtration and the solvent *in vacuo* gave a brown oil. The crude product was purified by silica gel chromatography (hexanes → hexanes : DCM (9 : 1)) to afford **1** as a light yellow oil (5.6460 g, 64.9%). ^{1}H NMR (400 MHz, acetone) δ 7.17 (t, J = 7.7 Hz, 2H), 7.12 (d, J = 7.6 Hz, 2H), 6.98 (d, J = 8.1 Hz, 2H), 6.92 (t, J = 7.5 Hz, 2H), 3.90 (t, J = 6.7 Hz, 2H), 1.83–1.71 (m, 2H), 1.50–1.38 (m, 2H), 1.35–1.18 (m, 12H), 0.87 (t, J = 6.7 Hz, 3H). ^{13}C NMR (101 MHz, $CDCl_3$) δ 145.31, 127.37, 127.12, 124.97, 122.27, 115.37, 47.38, 31.96, 29.61, 29.55, 29.36, 29.30, 26.97, 26.91, 22.76, 14.22. MS (ESI HRMS) m/z calcd for $C_{22}H_{29}NS$ + H: 340.2099; found 340.2071.

2a: 3,7-Dibromo-10-decyl-10*H*-phenothiazine. A solution of **1** (3.8843 g, 11.4 mmol) in $CHCl_3$: AcOH (1 : 1, 750 mL) was cooled in an ice bath and shielded from direct light. NBS (5.4973 g, 30.9 mmol) was then added in three equal portions with an hour between each addition. One hour after the last addition of NBS, water was added when the reaction mixture was still cold. The organic layer was removed, washed with H_2O until the washes were neutral and dried with magnesium sulfate to give a red oil once the solvent was removed *in vacuo*. Further purification with silica gel chromatography hexanes : DCM (9 : 1) gave **2a** as a light yellow

oil (2.7872 g, 49.0%). ^{1}H NMR (400 MHz, $CDCl_3$) δ 7.21 (dd, J = 8.6, 2.3 Hz, 2H), 7.18 (d, J = 2.2 Hz, 2H), 6.65 (d, J = 8.6 Hz, 2H), 3.79–3.66 (m, 2H), 1.79–1.68 (m, 2H), 1.45–1.35 (m, 2H), 1.35–1.22 (m, 12H), 0.92 (t, J = 6.9 Hz, 3H). ^{13}C NMR (101 MHz, $CDCl_3$) δ 143.79, 129.89, 129.40, 126.16, 116.39, 114.54, 47.40, 31.78, 29.41, 29.36, 29.18, 29.05, 26.66, 26.47, 22.60, 14.10. MS (ESI HRMS) m/z calcd for $C_{22}H_{27}Br_2NS$ + H: 496.0304; found 496.0308.

2b: 3,7-Dibromo-10-decyl-5-oxide-10*H*-phenothiazine. A solution of **2a** (1.0751 g, 2.16 mmol) and $Cu(NO_3)_2{\cdot}2.5H_2O$ (1.4297 g, 6.15 mmol) in DCM (40 mL) was sonicated under ambient conditions for 1 hour. The solid residue was removed by filtration and the solvent was removed *in vacuo* to afford a yellow mixture. The crude product was purified by silica gel column chromatography DCM : EtOAc (9 : 1) to give **2b** as a light beige oil that solidifies upon standing (0.6849 g, 61.5%). ^{1}H NMR (400 MHz, $CDCl_3$) δ 8.01 (d, J = 2.4 Hz, 2H), 7.68 (dd, J = 9.0, 2.4 Hz, 2H), 7.27 (d, J = 9.1 Hz, 2H), 4.16–4.09 (m, 2H), 1.94–1.83 (m, 2H), 1.53–1.44 (m, 2H), 1.44–1.22 (m, 12H), 0.89 (t, J = 6.9 Hz, 3H). ^{13}C NMR (101 MHz, $CDCl_3$) δ 137.03, 135.82, 133.67, 125.83, 117.70, 114.01, 48.50, 31.96, 29.65, 29.59, 29.37, 29.33, 26.84, 26.33, 22.77, 14.23. MS (ESI HRMS) m/z calcd for $C_{22}H_{27}Br_2NOS$ + H: 512.0258; found 512.0249.

2c: 3,7-Dibromo-10-decyl-5,5-dioxide-10*H*-phenothiazine. A solution of **2a** (0.5040 g, 1.01 mmol) in DCM (10 mL) was cooled in an ice bath before addition of mCPBA (75%, 0.7944 g, 3.45 mmol). The reaction mixture was stirred overnight as the temperature was allowed to slowly rise to room temperature. The crude product was purified by silica gel column chromatography (DCM) to give **2c** as a light brown oil (0.4317 g, 80.5%). ^{1}H NMR (400 MHz, $CDCl_3$) δ 8.16 (d, J = 2.4 Hz, 2H), 7.67 (dd, J = 9.1, 2.4 Hz, 2H), 7.20 (d, J = 9.1 Hz, 2H), 4.11–4.02 (m, 2H), 1.89–1.78 (m, 2H), 1.47–1.37 (m, 2H), 1.37–1.19 (m, 12H), 0.87 (t, J = 6.8 Hz, 3H). ^{13}C NMR (101 MHz, $CDCl_3$) δ 139.64, 136.27, 126.23, 125.51, 118.15, 114.46, 48.75, 31.94, 29.57, 29.53, 29.33, 29.22, 26.79, 26.63, 22.75, 14.22. MS (ESI HRMS) m/z calcd for $C_{22}H_{27}Br_2NO_2S$ + Na: 550.0021; found 550.0020.

3a: 4,4′-(10-Decyl-10*H*-phenothiazine-3,7-diyl)bis(ethyne-2,1-diyl)bis(*N*,*N*-didecylaniline). A yellow mixture of **2a** (0.5104 g, 1.03 mmol), bis(triphenylphosphine)palladium(II) dichloride (0.1539 g, 0.22 mmol), triphenyl phosphine (0.1714 g, 0.65 mmol) and copper(I) iodide (0.0713 g, 0.37 mmol) in dry triethylamine (25 mL) was purged with N_2. A sparged solution of **7** (1.2258 g, 3.08 mmol) in triethylamine (22 mL) was added using a syringe at the rate of 0.02 mL min^{-1} and left to stir for 2 weeks. Additional sparged dry triethylamine (25 ml) was added to reconstitute the solvent volume, then a second portion of a sparged solution of **7** (1.4430 g, 3.62 mmol) in dry triethylamine (22 mL) was added by syringe at a rate of 0.02 mL min^{-1} and stirred for 2 days. The solvent was removed *in vacuo* and the crude product was purified using silica gel chromatography hexanes : DCM (9 : 1 → 3 : 1) to yield a viscous yellow oil (0.6493 g, 55.7%). ^{1}H NMR (400 MHz, $CDCl_3$) δ 7.34 (d, J = 8.9 Hz, 4H), 7.30–7.24 (m, 2H), 7.23 (d, J = 1.9 Hz, 2H), 6.75 (d, J = 8.5 Hz, 2H), 6.57 (d, J = 9.0 Hz, 4H), 3.81 (t, J = 7.1 Hz, 2H), 3.36–3.20 (m, 8H), 1.86–1.73 (m, 2H), 1.64–1.53 (m, 8H), 1.48–1.38 (m, 2H), 1.38–1.21 (m, 68H), 0.95–0.86 (m, 15H). ^{13}C NMR (101 MHz, $CDCl_3$) δ 147.82, 143.95, 132.71, 130.30, 129.81, 124.09, 118.36, 114.98, 111.21, 108.86, 90.64, 86.26, 50.97, 47.62, 31.89, 29.65, 29.56, 29.51, 29.31, 29.20, 27.22, 27.14, 26.82, 22.67, 14.10. MS (ESI HRMS) m/z calcd for $C_{78}H_{119}N_3S$ + H: 1130.9197; found 1130.9192.

3b: 4,4′-(10-Decyl-5-oxide-10*H*-phenothiazine-3,7-diyl)bis(ethyne-2,1-diyl)bis(*N*,*N*-didecylaniline). A yellow mixture of **2b** (0.3904 g, 0.76 mmol), bis(triphenylphosphine)palladium(II) dichloride (0.0535 g, 0.076 mmol), triphenyl phosphine (0.0600 g, 0.23 mmol) and copper(I) iodide (0.0310 g, 0.16 mmol) in dry triethylamine (24 mL) was purged with N_2. A sparged solution of **7** (0.9960 g, 2.3 mmol) in triethylamine (22 mL) was added by syringe at a rate of 0.02 mL min^{-1} while the mixture was stirred under N_2. The solvent was removed from the brown mixture *in vacuo* and the crude oil was purified using silica gel chromatography DCM : EtOAc (99 : 1) to give **3b** as a golden oil (0.2941 g, 33.7%). **3b** is fairly stable in air but when exposed to light while in solution, it decomposes to a deep green substance. ^{1}H NMR (400 MHz, $CDCl_3$) δ 8.06 (d, J = 2.0 Hz, 2H), 7.69 (dd, J = 8.8, 2.0 Hz, 2H), 7.39 (d, J = 8.8 Hz, 4H), 7.32 (d, J = 9.0 Hz, 2H), 6.59 (d, J = 9.0 Hz, 4H), 4.22–4.10 (m, 2H), 3.35–3.22 (m, 8H), 2.00–1.86 (m, 2H), 1.66–1.55 (m, 8H), 1.55–1.47 (m, 2H), 1.47–1.39 (m, 2H), 1.39–1.23 (m, 66H), 0.96–0.87 (m, 15H). ^{13}C NMR (101 MHz, $CDCl_3$) δ 147.93, 136.58, 135.25, 134.35, 132.79, 124.11, 118.14, 115.60, 111.15, 108.33, 91.79, 85.55, 50.90, 31.83, 29.60, 29.51, 29.46, 29.25, 29.21, 27.16, 27.07, 26.73, 22.63, 14.06. MS (ESI HRMS) m/z calcd for $C_{78}H_{119}N_3SO$ + H: 1146.9147; found 1146.9120.

3c: 4,4′-(10-Decyl-5,5-dioxide-10*H*-phenothiazine-3,7-diyl)bis(ethyne-2,1-diyl)bis(*N*,*N*-didecylaniline). A yellow mixture of **2c** (0.3039 g, 0.57 mmol), bis(triphenylphosphine)palladium(II) dichloride (0.0445 g, 0.063 mmol), triphenyl phosphine (0.0472 g, 0.18 mmol) and copper(I) iodide (0.0193 g, 0.10 mmol) in dry triethylamine (25 mL) was purged with N_2. A sparged solution of **7** (0.7010 g, 1.76 mmol) in triethylamine (22 mL) was added using a syringe at the rate of 0.02 mL min^{-1} while the mixture was stirred under N_2. The solvent was removed from the brown mixture *in vacuo* and the crude product was purified using silica column chromatography hexanes : DCM (2 : 3) to give a yellow oil that solidifies upon standing (0.4242 g, 63.6%). ^{1}H NMR (400 MHz, $CDCl_3$) δ 8.24 (d, J = 2.0 Hz, 2H), 7.65 (dd, J = 8.9, 1.2 Hz, 2H), 7.37 (d, J = 8.9 Hz, 4H), 7.23 (d, J = 9.0 Hz, 2H), 6.58 (d, J = 9.0 Hz, 4H), 4.15–4.03 (m, 2H), 3.35–3.22 (m, 8H), 1.98–1.80 (m, 2H), 1.67–1.52 (m, 8H), 1.51–1.42 (m, 2H), 1.42–1.22 (m, 68H), 0.90 (t, J = 6.8 Hz, 15H). ^{13}C NMR (101 MHz, $CDCl_3$) δ 148.09, 138.90, 135.38, 132.89, 126.27, 124.19, 118.46, 115.95, 111.19, 108.14, 92.44, 85.32, 50.94, 31.87, 31.84, 29.63, 29.54, 29.49, 29.45, 29.29, 29.25, 29.15, 27.20, 27.11, 26.73, 26.60, 22.65, 14.08. MS (ESI HRMS) m/z calcd for $C_{78}H_{119}N_3SO_2$ + H: 1162.9096; found 1162.9092.

Electrochemistry

Cyclic voltammetry (CV) experiments were carried out on an Autolab PGSTAT302 potentiostat that was controlled by a PC running Autolab's GPES v 4.9 software in a temperature- controlled, three-electrode cell (15 mL). The working electrode was a Pt button,

the reference electrode was a silver wire and the counter electrode was a Pt wire. All potentials were referenced to the ferrocene/ferricenium redox couple. Each CV experiment consisted of approximately 2–5 mM redox active species dissolved in 0.05 M tetrabutylammonium hexafluorophosphate in deoxygenated DMF. All CV solutions were sparged with Ar prior to dissolving the redox active species and an Ar blanket was maintained during the entire experiment. Spectroelectrochemical spectra were generated on a Cary 5000 spectrophotometer linked with a CHI 650 potentiostat using a thin layer cell (OTTLE). The working electrode, in the beam path, was a Pt mesh, a Pt wire counter electrode and a silver wire reference electrode; electrolyte and solvent were used as above.

Acknowledgements

The authors thank the NSERC Discover Grants program and KDT thanks NSERC and Alberta Innovates – Technology Futures for a postgraduate scholarship.

Notes and references

1 J. H. Stebbins Jr., *J. Am. Chem. Soc.*, 1884, **6**, 304–305.
2 J. Guan, D. E. Kyle, L. Gerena, Q. Zhang, W. K. Milhous and A. J. Lin, *J. Med. Chem.*, 2002, **45**, 2741–2748.
3 M. Viveiros and L. Amaral, *Int. J. Antimicrob. Agents*, 2001, **17**, 225–228.
4 M. Lee, J. E. Park, C. Park and H. C. Choi, *Langmuir*, 2013, **29**, 9967–9971.
5 A. S. Hart, K. C. Chandra Bikram, N. K. Subbaiyan, P. A. Karr and F. D'Souza, *ACS Appl. Mater. Interfaces*, 2012, **4**, 5813–5820.
6 A. Tacca, R. Po, M. Caldararo, S. Chiaberge, L. Gila, L. Longo, P. R. Mussini, A. Pellegrino, N. Perin, M. Salvalaggio, A. Savoini and S. Spera, *Electrochim. Acta*, 2011, **56**, 6638–6653.
7 Z. Wan, C. Jia, Y. Duan, J. Zhang, Y. Lin and Y. Shi, *Dyes Pigm.*, 2012, **94**, 150–155.
8 F. Xu, C. Wang, L. Yang, S. Yin, A. Wedel, S. Janietz, H. Krueger and Y. Hua, *Synth. Met.*, 2005, **152**, 221–224.
9 C. S. Barkschat, S. Stoycheva, M. Himmelhaus and T. J. J. Mueller, *Chem. Mater.*, 2010, **22**, 52–63.
10 N. Bucci and T. J. J. Mueller, *Tetrahedron Lett.*, 2006, **47**, 8329–8332.
11 C. S. Kraemer and T. J. J. Mueller, *Eur. J. Org. Chem.*, 2003, 3534–3548.
12 C. S. Kraemer, K. Zeitler and T. J. J. Mueller, *Org. Lett.*, 2000, **2**, 3723–3726.
13 X. Ma, X. Mao, S. Zhang, X. Huang, Y. Cheng and C. Zhu, *Polym. Chem.*, 2013, **4**, 520–527.
14 T. J. J. Muller, *Tetrahedron Lett.*, 1999, **40**, 6563–6566.
15 M. Song, J. S. Park, Y. H. Kim, M. A. Karim, S.-H. Jin, R. S. Ree, Y. R. Cho, Y.-S. Gal and J. W. Lee, *Macromol. Res.*, 2011, **19**, 654–659.
16 W.-Y. Wong, W.-C. Chow, K.-Y. Cheung, M.-K. Fung, A. B. Djurisic and W.-K. Chan, *J. Organomet. Chem.*, 2009, **694**, 2717–2726.
17 W.-W. Zhang, W.-L. Mao, Y.-X. Hu, Z.-Q. Tian, Z.-L. Wang and Q.-J. Meng, *J. Phys. Chem. A*, 2009, **113**, 9997–10004.
18 W.-W. Zhang, Y.-G. Yu, Z.-D. Lu, W.-L. Mao, Y.-Z. Li and Q.-J. Meng, *Organometallics*, 2007, **26**, 865–873.
19 Y. Zhu, A. P. Kulkarni, P.-T. Wu and S. A. Jenekhe, *Chem. Mater.*, 2008, **20**, 4200–4211.
20 T. Agou, J. Kobayashi and T. Kawashima, *Chem. Commun.*, 2007, 3204–3206.
21 T. Agou, T. Kojima, J. Kobayashi and T. Kawashima, *Org. Lett.*, 2009, **11**, 3534–3537.
22 S. G. Dahl, E. Hough and P.-A. Hals, *Biochem. Pharmacol.*, 1986, **35**, 1263–1269.
23 K. T. Kamtekar, K. Dahms, A. S. Batsanov, V. Jankus, H. L. Vaughan, A. P. Monkman and M. R. Bryce, *J. Polym. Sci., Part A: Polym. Chem.*, 2011, **49**, 1129–1137.
24 C. S. Krämer and T. J. J. Müller, *Eur. J. Org. Chem.*, 2003, 3534–3548.
25 C. S. Krämer, K. Zeitler and T. J. J. Müller, *Org. Lett.*, 2000, **2**, 3723–3726.
26 T. Okuno, S. Ikeda, N. Kubo and D. J. Sandman, *Mol. Cryst. Liq. Cryst.*, 2006, **456**, 35–44.
27 S. Umezono and T. Okuno, *Acta Crystallogr., Sect. E: Struct. Rep. Online*, 2012, **68**, o2790.
28 W.-W. Zhang, Y.-G. Yu, Z.-D. Lu, W.-L. Mao, Y.-Z. Li and Q.-J. Meng, *Organometallics*, 2007, **26**, 865–873.
29 S. S. C. Chu, P. De Meester, M. V. Jovanovic and E. R. Biehl, *Acta Crystallogr., Sect. C: Cryst. Struct. Commun.*, 1985, **41**, 1111–1114.
30 E. Hough, M. Hjorth and S. G. Dahl, *Acta Crystallogr., Sect. B: Struct. Crystallogr. Cryst. Chem.*, 1982, **38**, 2424–2428.
31 H. Tabata and T. Okuno, *Acta Crystallogr., Sect. E: Struct. Rep. Online*, 2012, **68**, o2214.
32 S. Umezono, S. Ikeda and T. Okuno, *Acta Crystallogr., Sect. C: Cryst. Struct. Commun.*, 2013, **69**, 1553–1556.
33 S. Umezono and T. Okuno, *J. Mol. Struct.*, 2013, **1049**, 293–298.
34 Z. Xu, Y. Sun, L. Yang and Q. Wang, *Acta Crystallogr., Sect. E: Struct. Rep. Online*, 2009, **65**, o1799.
35 M. S. Siddegowda, R. J. Butcher, M. Akkurt, H. S. Yathirajan and A. R. Ramesh, *Acta Crystallogr., Sect. E: Struct. Rep. Online*, 2011, **67**, o1875.
36 M. S. Siddegowda, J. P. Jasinski, J. A. Golen and H. S. Yathirajan, *Acta Crystallogr., Sect. E: Struct. Rep. Online*, 2011, **67**, o1702.
37 H. Tabata and T. Okuno, *Acta Crystallogr., Sect. E: Struct. Rep. Online*, 2012, **68**, o2519.
38 M. Sailer, A. W. Franz and T. J. J. Müller, *Chem. – Eur. J.*, 2008, **14**, 2602–2614.
39 S. A. Elkassih, P. Sista, H. D. Magurudeniya, A. Papadimitratos, A. A. Zakhidov, M. C. Biewer and M. C. Stefan, *Macromol. Chem. Phys.*, 2013, **214**, 572–577.
40 S.-K. Son, Y.-S. Choi, W.-H. Lee, Y. Hong, J.-R. Kim, W.-S. Shin, S.-J. Moon, D.-H. Hwang and I.-N. Kang, *J. Polym. Sci., Part A: Polym. Chem.*, 2010, **48**, 635–646.
41 L. Gaina, A. Csampai, G. Turos, T. Lovasz, V. Zsoldos-Mady, I. A. Silberg and P. Sohar, *Org. Biomol. Chem.*, 2006, **4**, 4375–4386.

42 T. Ishihara, H. Kakuta, H. Moritani, T. Ugawa and I. Yanagisawa, *Chem. Pharm. Bull.*, 2004, **52**, 1204–1209.
43 M. Hauck, M. Stolte, J. Schönhaber, H.-G. Kuball and T. J. J. Müller, *Chem. – Eur. J.*, 2011, **17**, 9984–9998.
44 L. Yang, J.-K. Feng and A.-M. Ren, *J. Org. Chem.*, 2005, **70**, 5987–5996.
45 J. Catalán, *J. Phys. Chem. B*, 2009, **113**, 5951–5960.
46 J. Catalán and C. Díaz, *Liebigs Ann.*, 1997, **1997**, 1941–1949.
47 J. Catalán, C. Díaz, V. López, P. Pérez, J.-L. G. De Paz and J. G. Rodríguez, *Liebigs Ann.*, 1996, **1996**, 1785–1794.
48 M. J. Kamlet and R. W. Taft, *J. Am. Chem. Soc.*, 1976, **98**, 377–383.
49 R. W. Taft and M. J. Kamlet, *J. Am. Chem. Soc.*, 1976, **98**, 2886–2894.
50 V. Gutmann, *Coord. Chem. Rev.*, 1976, **18**, 225–255.
51 R. S. Drago, *Applications of Electrostatic-covalent Models in Chemistry*, Surfside Scientific Publishers, 1994.
52 J. G. Kirkwood, *J. Chem. Phys.*, 1934, **2**, 351–361.
53 L. Onsager, *J. Am. Chem. Soc.*, 1936, **58**, 1486–1493.
54 D. C. Dong and M. A. Winnik, *Can. J. Chem.*, 1984, **62**, 2560–2565.
55 M. J. Kamlet, J. L. Abboud and R. W. Taft, *J. Am. Chem. Soc.*, 1977, **99**, 6027–6038.
56 R. S. Drago, *J. Chem. Soc., Perkin Trans. 2*, 1992, 1827–1838.
57 J. Catalán, V. López, P. Pérez, R. Martin-Villamil and J.-G. Rodríguez, *Liebigs Ann.*, 1995, **1995**, 241–252.
58 M. J. Frisch, G. W. Trucks, H. B. Schlegel, G. E. Scuseria, M. A. Robb, J. R. Cheeseman, G. Scalmani, V. Barone, B. Mennucci, G. A. Petersson, H. Nakatsuji, M. Caricato, X. Li, H. P. Hratchian, A. F. Izmaylov, J. Bloino, G. Zheng, J. L. Sonnenberg, M. Hada, M. Ehara, K. Toyota, R. Fukuda, J. Hasegawa, M. Ishida, T. Nakajima, Y. Honda, O. Kitao, H. Nakai, T. Vreven, J. A. Montgomery, J. E. Peralta, F. Ogliaro, M. Bearpark, J. J. Heyd, E. Brothers, K. N. Kudin, V. N. Staroverov, R. Kobayashi, J. Normand, K. Raghavachari, A. Rendell, J. C. Burant, S. S. Iyengar, J. Tomasi, M. Cossi, N. Rega, J. M. Millam, M. Klene, J. E. Knox, J. B. Cross, V. Bakken, C. Adamo, J. Jaramillo, R. Gomperts, R. E. Stratmann, O. Yazyev, A. J. Austin, R. Cammi, C. Pomelli, J. W. Ochterski, R. L. Martin, K. Morokuma, V. G. Zakrzewski, G. A. Voth, P. Salvador, J. J. Dannenberg, S. Dapprich, A. D. Daniels, Ö. Farkas, J. B. Foresman, J. V. Ortiz, J. Cioslowski and D. J. Fox, Gaussian, Inc., Wallingford, CT, 2009.
59 S. Trasatti, *Pure Appl. Chem.*, 1986, **58**, 955–966.
60 T. Le Bahers, T. Pauporte, G. Scalmani, C. Adamo and I. Ciofini, *Phys. Chem. Chem. Phys.*, 2009, **11**, 11276–11284.
61 A. Pedone, J. Bloino, S. Monti, G. Prampolini and V. Barone, *Phys. Chem. Chem. Phys.*, 2010, **12**, 1000–1006.
62 D. Pan and D. L. Phillips, *J. Phys. Chem. A*, 1999, **103**, 4737–4743.

